Bio-Design and Manufacturing (2025) 8:331–343
https://doi.org/10.1631/bdm.2400005

RESEARCH ARTICLE

Biomimetically neurovascularized engineered muscle tissue for craniofacial volumetric muscle loss

Sijia Ding[1,2] · Shengjie Li[1,2] · Zhuojie Shen[1,2] · Yuhua Chen[1,2] · Xia Wang[1,2] · Jianxiang He[1,2] · Huiming Wang[1,2] · Mengfei Yu[1,2]

Received: 3 January 2024 / Accepted: 14 September 2024

Abstract

Craniofacial muscles are essential components of the skeletal muscular system that contribute to important physiological processes. Severe trauma can induce craniofacial volumetric muscle loss (VML), which impairs muscle regeneration, causes facial muscular deformities and functional disability, and leads to psychosocial consequences such as isolation and depression. Conventional therapies involving muscle flap transposition or autologous tissue grafting achieve morphological repair but are ineffective in restoring muscle function, resulting in donor site injury and sensory deficit. In this study, we successfully constructed a biomimetically engineered muscle tissue that integrates myofiber alignment, effective innervation, and blood perfusion to promote multi-tissue regeneration in the masseter area in vivo, enabling functional regeneration. Using light-controlled micropatterning technology, we constructed mature muscle fibers with oriented alignment and established a neuromuscular co-culture system for in vitro neuromuscular junction reconstruction. Furthermore, we designed and fabricated a vascular network structure to promote tissue vascularization using hydrogel as the vehicle for assembling the composite engineered tissue. Using this technology, the shape and dimension of the constructed entity can be customized to address various muscle defects, enabling individualized repair. This study offers a promising novel strategy for tissue regeneration that breaks through the current challenges in the treatment of craniofacial VML.

Sijia Ding, Shengjie Li, and Zhuojie Shen have contributed equally to this work.

✉ Jianxiang He
hejianxiang@zju.edu.cn

✉ Huiming Wang
whmwhm@zju.edu.cn

✉ Mengfei Yu
yumengfei@zju.edu.cn

[1] The Affiliated Hospital of Stomatology, School of Stomatology, Zhejiang University School of Medicine, Hangzhou 310006, China

[2] Key Laboratory of Oral Biomedical Research of Zhejiang Province, Hangzhou 310006, China

Graphical abstract

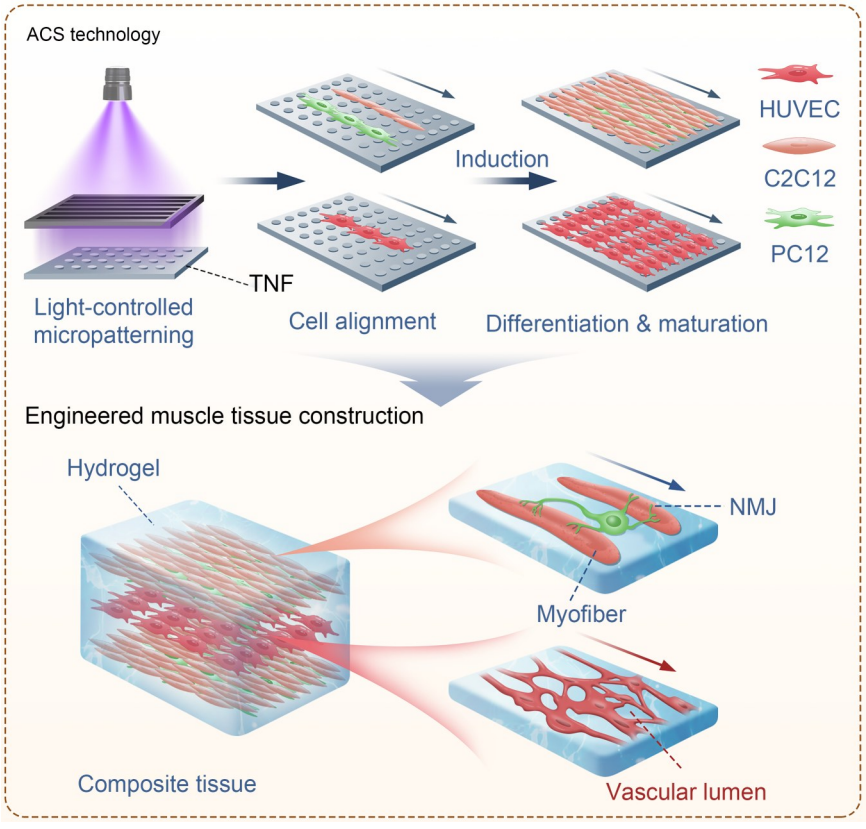

Keywords Tissue engineering · Biomimetics · Masticatory muscles · Biomaterials · Regenerative medicine

1 Introduction

Skeletal muscle is the most abundant tissue in the human body, accounting for approximately 40% of the total body mass [1]. It is mainly involved in locomotion and metabolism [2]. Skeletal muscles are classified into three main groups based on location and function: trunk muscles, head and neck muscles, and limb muscles. Head muscles differ from other muscle groups in their distinct origins and development, as well as the underlying regulatory cascades [3, 4]. While not required for locomotion, the head skeletal muscles function in food uptake, respiration, control over the cranial opening, and vision, which are all crucial for survival [5]. In addition, the masticatory muscle, a prominent head muscle [6], can generate occlusal pressure with great force while enabling extremely precise movement control [7]. Such specialized physiological and functional features maintain the pressure balance of the muscles and dentition in the maxillofacial region, which are essential for maintaining symmetrical facial morphology and normal occlusal relations [8].

Severe trauma can cause volumetric muscle loss (VML), which can impair muscle regeneration and lead to persistent atrophy [9–11]. The extensive defect resulting from VML can be addressed by current clinical treatments, such as muscle flap transposition or autologous tissue grafting. However, such improvements are mostly cosmetic and can come with complications, such as donor site morbidity and sensory deficits [12]. These methods can achieve morphologic repair but are ineffective in improving muscle structure and function [13]. Furthermore, the lack of satellite cells in the masticatory muscle region may explain the poor regenerative ability in response to acute damage [14, 15], making treatment of craniofacial VML more challenging. Therefore, the development of a novel tissue engineering strategy that can achieve both morphological and functional muscle repair is highly desired.

In its natural state, masticatory muscle exhibits distinct structural characteristics and unique physiological functions [7]. It consists of numerous organized muscle fibers that can contract in a controlled and directed manner to generate force, serving as the foundation for muscular

contractive functions [16, 17]. In addition, routine chewing and articulating functions require muscles with great occlusal strength and precise occlusal position [18]. Thus, modulating myoblast alignment is crucial in tissue engineering to achieve the functional recovery of masticatory muscles. Furthermore, neuralization and vascularization are inextricably linked to physiological muscle function and long-term survival. Effective innervation is essential for muscle signaling [19]; denervation of skeletal muscle can lead to atrophy within three weeks, progressing to irreversible fibrosis after two years without reinnervation [20]. Furthermore, an abundant blood supply is essential for sustaining high muscular metabolic activity and the delivery of vital nutrients and oxygen [21]. Although current engineering strategies can facilitate muscle regeneration, their capacity for repairing surrounding nerves and vessels is significantly limited.

This study aimed to bridge the research gap in tissue engineering for repairing craniofacial VML. We successfully constructed mature muscle fibers with a specified orientation and established a neuromuscular co-culture system that enables in vitro neuromuscular junction (NMJ) reconstruction. A mature vascular network structure was also constructed, using hydrogel as the vehicle for assembling the three-dimensional (3D) neurovascularized engineered muscle tissue. This construct precisely mimics the structure and characteristics of natural muscle and can promote multitissue regeneration in the masseter area in vivo (Fig. 1). Therefore, the results of this study demonstrate a potential

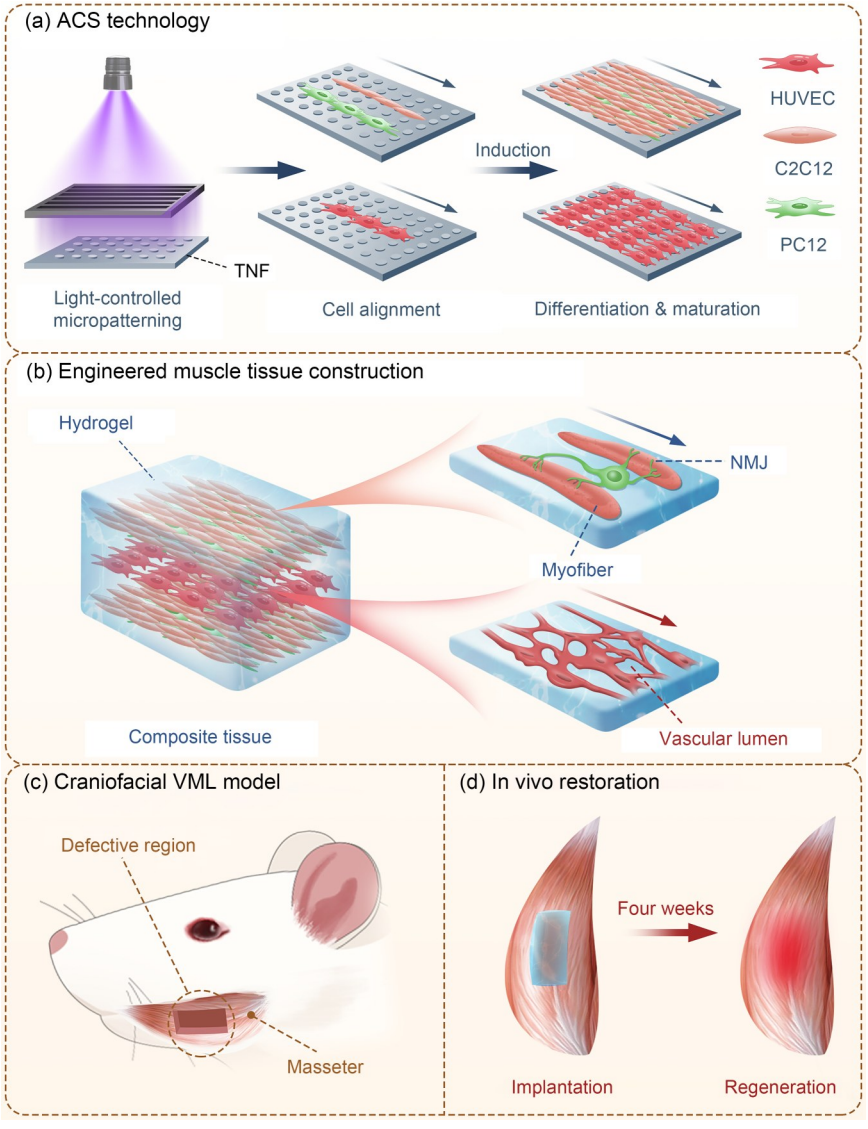

Fig. 1 Schematic diagram of the fabrication of biomimetically neurovascularized engineered muscle tissue used to repair craniofacial volumetric muscle loss. (a) ACS technology regulates cell alignment and induces differentiation and maturation. (b) Construction of hydrogel-based composite engineered muscle tissue. (c) Construction of a craniofacial VML mouse model. (d) In vivo restoration of the masseter muscle. ACS: anisotropic cell sheets; TNF: TiO_2 nanodot film; HUVEC: human umbilical vein endothelial cell

novel therapeutic strategy for neurovascularized muscle regeneration in craniofacial muscle tissue engineering.

2 Materials and methods

2.1 TiO_2 nanodot film (TNF) preparation and ultraviolet (UV)-controlled cell alignment

TNFs were prepared on the surface of quartz substrates using a phase separation-induced self-assembly approach, as previously reported [22]. First, a precursor sol consisting of a mixture of tetrabutyl titanate (Sinopharm Chemical Reagents, Beijing, China), acetylacetone (Lingfeng Chemical Reagents, Shanghai, China), and polyvinylpyrrolidone (Sinopharm Chemical Reagents) was prepared and spin-coated onto the surface of the quartz substrate (10 mm× 10 mm×1 mm). Then, the substrates were heat-treated at 500 °C for 1 h. After autoclaving and drying, the TNFs were stored in a dark room before subsequent cell culture.

The UV micropatterning of TNFs was performed with a designed photomask, as previously reported [23]. A UV light source (254 nm, 300 μW/cm^2) was used to irradiate UV light through the photomask to form micropatterns of parallel lines with a width spacing of 30 μm. The TNFs were then immediately moved to the well plate with tweezers, and cells were added to the substrate for alignment along the micropattern.

2.2 Cell culture

The C2C12, PC12, and human umbilical vein endothelial cells (HUVECs) were purchased from the American Type Culture Collection (ATCC, Rockville, MD, USA). C2C12 and PC12 cells were cultured in Dulbecco's modified Eagle's medium (DMEM; high glucose) with 10% fetal bovine serum (FBS) according to the instructions. HUVECs were cultured in a vascular cell basal medium supplemented with an endothelial cell growth kit—vascular endothelial growth factor (VEGF; ATCC).

All the cells were incubated at 37 °C under an atmosphere of 5% CO_2. Media were replaced every 2 d, and cells were harvested at 80% confluence. C2C12 cells (1× 10^5 cells/well) were seeded onto each TNF and cultured in DMEM with 10% FBS. To construct the differentiated myotubes, the growth medium was changed to myogenic differentiation medium (DMEM; high glucose containing 2% horse serum) after 24 h to further induce differentiation for 7 d.

2.3 In vitro contractional testing

Polyvinylidene fluoride (PVDF) was used to transfer cells in Align and Non-align groups. A PVDF sheet was cut into 1 cm×1 cm pieces and attached to the cells cultured on the TNF. After 1 min of exposure to UV light, the cell sheet was transferred to the PVDF surface. An electrical stimulator (BEX, Tokyo, Japan) with two electrodes connected to each end of the material was used to induce cell contraction. Following electrical stimulation with the same parameters for each group, the bending angle of the PVDF sheet was promptly measured.

2.4 Co-culture system

The C2C12 and PC12 cells were counted, and the two cell suspensions were pre-mixed at specific ratios (1:0, 30:1, 50:1, 70:1, 100:1, and 300:1) and added into 24-well plates for co-culture. The growth medium (DMEM; high glucose containing 10% FBS) was selected on the first day and replaced with differentiation medium (DMEM; high glucose containing 2% horse serum and 50 ng/mL nerve growth factor) on the second day. Subsequently, cells were collected for evaluation after 7 d of co-culture.

2.5 Immunofluorescent staining

Samples were fixed with 4% paraformaldehyde, permeabilized with 0.05% Triton X 100/phosphate-buffered saline, blocked with 2% bovine serum albumin solution, and incubated with the configured primary antibody solution at 4 °C overnight. The primary antibodies were myosin heavy chain (MHC) (sc376157, Santa Cruz, Dallas, TX, USA), beta-III tubulin (βIIIT) (ab18207, Abcam, Cambridge, MA, USA), and acetylcholine receptor (AChR) (ab41174, Abcam). On the next day, after rewarming and washing, the samples were incubated with the configured secondary antibody for 1 h. After washing off, the nuclei were stained with 4′,6-diamidino-2-phenylindole (DAPI). The secondary antibodies used were AlexaFluor 488-labeled IgG antibody (Dawen, Hangzhou, China) and AlexaFluor 594-labeled IgG antibody (Dawen). Filamentous actin (F-actin) cytoskeleton staining was performed using rhodamine–phalloidin (Cytoskeleton, Denver, CO, USA). Fluorescence was detected using an inverted fluorescence microscope (ThermoFisher Scientific, Waltham, MA, USA) and confocal laser scanning microscope (Nikon, Tokyo, Japan).

2.6 Preparation of GelMA hydrogel

The gelatin methacryloyl (GelMA) prepolymer solution was prepared at 10% concentration, as previously reported [23]. The GelMA solution was melted after heating and added to the fused cells on the TNF. The TNF and cells were then exposed to UV light from the bottom of the plate. After 1 min of illumination, the solidified GelMA was removed from the TNF with a blade, with cell sheets adhering to its

surface. The same strategy for preparing 3D multilayer structures was performed to further transfer and stack different cell sheets.

2.7 Construction of composite tissue

The PC12 and C2C12 cells were mixed and co-cultured on the TNF surface at the predetermined ratios. After 7 d of differentiation, the cells fused to form the neuromuscular layer. In addition, HUVECs formed a capillary-like network layer using the same method. The stacking and assembly of different layers of the engineered tissue were implemented sequentially in vitro using GelMA to make the layers stick to one another, forming a whole construct consisting of the upper and lower neuromuscular layers and a capillary-like vascular network middle layer.

2.8 Craniofacial VML nude mouse model

Masseter defects were established in eight-week-old immunodeficient male nude mice. Mice were anesthetized with sodium pentobarbital, after which the skin was cut to expose the masseter area. Approximately 40%–50% of the muscle volume was removed with a scalpel. Following hemostasis and cleaning, a suitable construct was selected according to the defect site and transplanted along the muscle fiber direction. GelMA was applied around the edge of the construct for adhesion and fixation after photocuring, ensuring that the engineered tissue was securely fixed in the target area. The mice were divided into the Sham (sham operation only), Defect (no treatment), Non-align (implantation of non-aligned construction), and Align (implantation of aligned construction) groups. The recovery of the mice in each group was evaluated after four weeks of implantation.

2.9 Histological analysis

Mice were euthanized four weeks after the operation with an overdose of sodium pentobarbital. The masseter muscles of the mice were isolated, collected, and fixed in 4% paraformaldehyde (Sigma-Aldrich, St. Louis, MO, USA). The tissues were dehydrated, embedded in paraffin, and sliced into eight-μm-thick slices. The paraffin slices in all groups were stained with hematoxylin–eosin (H&E) (Sigma-Aldrich) and Masson's trichrome (MT) (Sigma-Aldrich). Histological features were determined under microscopy. Areas of fibrosis were identified and quantified using the ImageJ software. Regarding tissue localization in the section, the target tissue area was located by referring to the site of the excised muscle. The remaining hydrogel and boundary between the hydrogel and the muscle tissue were described.

2.10 Functional evaluation

After surgery completion and four weeks of restoration, mice in each group were weighed, and differences in weight before and after surgery were analyzed. Following a 12-h fasting period, mice were provided with standard food in feeders, and the food intake within a fixed time frame (10 min) was recorded for each group.

2.11 Statistical analysis

All data were presented as mean±standard deviation (SD). For statistical analyses, one-way analysis of variance (ANOVA) or *t*-test was employed with the programs of GraphPad Prism and SPSS statistics. A *p*-value of less than 0.05 was considered statistically significant.

3 Results

3.1 Light-controlled micropatterning-induced cell alignment

To construct aligned cell sheets, a parallel-patterned mask was placed above the TNF, which was then subjected to UV light exposure for micropatterning. C2C12 myoblasts were then seeded onto the patterned TNF (Fig. 2a). These methods were performed as described in a previous study by our research group [23]. C2C12 cells were cultured separately on micropatterned and untreated TNF surfaces, designated as the Align and Non-align groups, respectively. Figure 2b shows cells that were cultured for 24 h and then subjected to immunofluorescence staining for F-actin to assess the cell orientation. Cells in the Align group were organized toward a defined direction, whereas cells in the Non-align group were disordered and randomly arranged. Quantitative analysis of cell orientation further confirmed the feasibility of this approach for implementing cell alignment (Fig. 2c). Using electrical stimulation to induce cell contraction, the unidirectional contraction of the myoblasts was compared between the two groups. The material containing the aligned cells could bend along one direction, whereas the material in the Non-align group showed less bending (Fig. 2d). Quantitative results also confirmed this discrepancy, indicating that cell alignment may enhance cell functionality (Fig. 2e).

3.2 Cell alignment promoting myogenic differentiation

Following induction in myogenic differentiation medium for 5 and 7 d, immunofluorescent staining for MHC was performed to label the differentiated and mature muscle

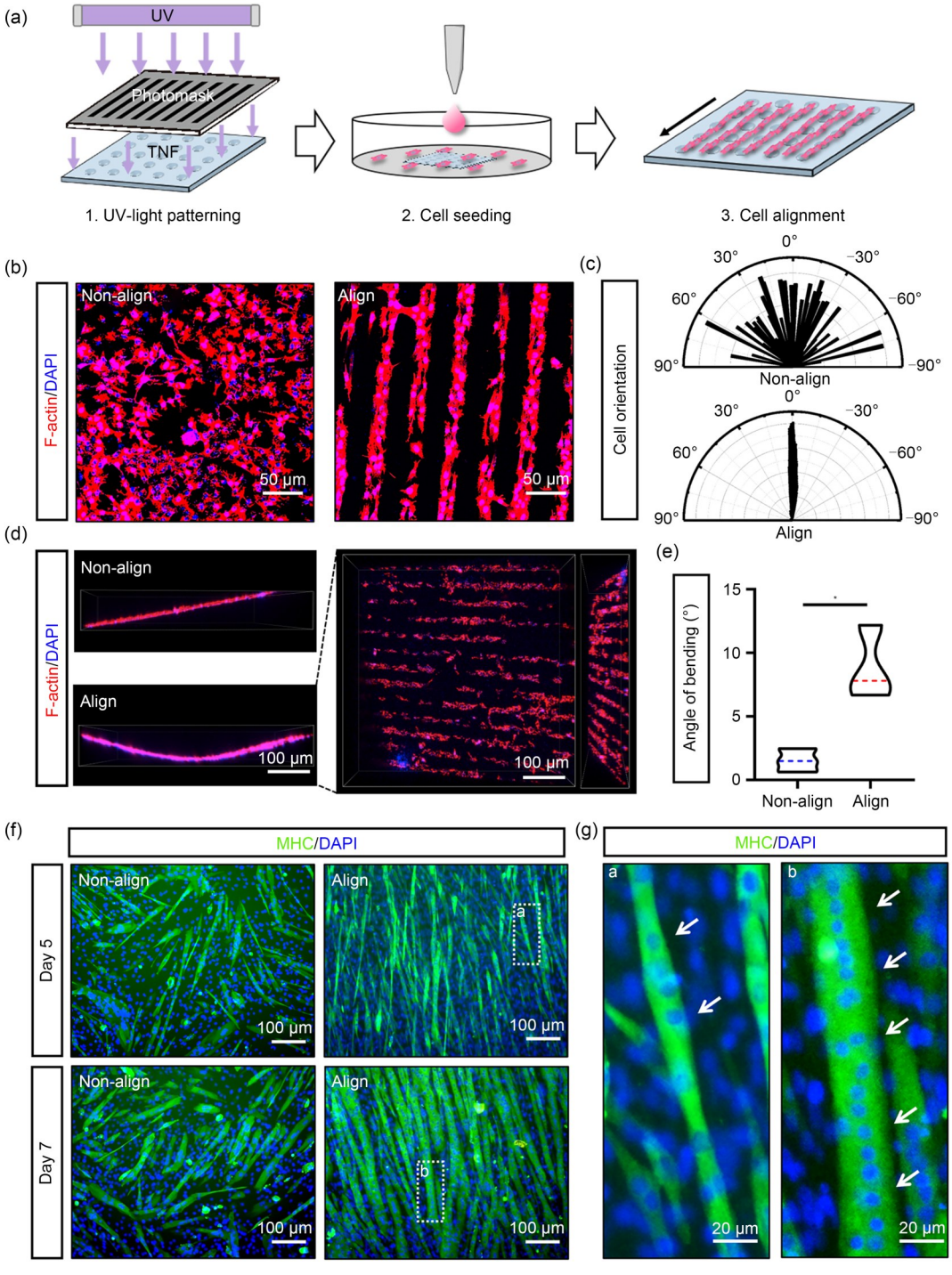

Fig. 2 Light-controlled micropatterning induces cell alignment and promotes myogenesis. (a) Schematic illustration of the procedure for light-controlled micropatterning to induce cell alignment. (b) Immunofluorescence for F-actin (red)/DAPI (blue) in C2C12 cells cultured in unpatterned and patterned TNFs (Non-align and Align groups, respectively) for 24 h. (c) Quantitative analysis of cell orientation in the two groups (n=20 per group). (d) Confocal microscopic images of z-stack, showing the bending of PVDFs carrying C2C12 cells under electrical stimulation. (e) Quantification of bending angle (n=5 per group). (f) Immunofluorescence for myogenic marker MHC (green)/DAPI (blue) of C2C12 cells after 5 and 7 d of myogenic differentiation. (g) Comparison of MHC+ multinuclear myotubes after 5 and 7 d of differentiation. All data are expressed as mean±standard deviation, $^{*}p<0.05$; t-test was employed. MHC+: MHC-positive

fibers. Muscle fibers formed in the Align group encompassed a greater area and diameter than those in the Non-align group (Fig. 2f). Furthermore, in the Align group, more fused nuclei were observed on Day 7 after induction than those on Day 5, signifying increasing maturity of structural development (Fig. 2g). This result is further supported by the

quantitative analysis of myofiber length and nuclear fusion in each group (Fig. S1 in the supplementary information). Based on these findings, we confirmed that myoblast alignment can promote myogenic differentiation, with longer periods of aligned culture yielding more favorable myogenic outcomes.

3.3 Neuron–muscle cell co-culture system

To further accelerate the neural innervation of muscle tissue, we added PC12 cells to the C2C12 cell culture in a two-dimensional (2D) system. We selected six different co-culture ratios and compared the myogenic differentiation outcomes among the different co-cultures. The immunofluorescent results demonstrated a notable increase in myofiber formation at a C2C12:PC12 ratio of 100:1 compared to the C2C12-only group (Fig. 3a). The quantitative analysis also confirmed that larger myofiber area and greater width were attained (Figs. 3b and 3c). Furthermore, when the C2C12:PC12 ratio was below 70:1, with a higher proportion of PC12, the myofiber area decreased, indicating that an excess of non-myogenic cells hindered myogenesis. Therefore, to optimize myogenic differentiation conditions, subsequent experiments involving neuromuscular cell co-culture used a 100:1 ratio.

3.4 Construction of aligned neurovascularized engineered tissue

Using the light-controlled cell alignment technique, we constructed two structures: an aligned neuromuscular layer and a vascular network layer. Predetermined proportions of neuromuscular co-cultured cells were added and arranged in alignment. After 7 d of differentiation, both the neuromuscular and vascular network layers exhibited mature morphology. Specifically, C2C12 cells fused and differentiated into multi-nucleated myotubes, while PC12 cells were distributed around the myotubes, demonstrating the differentiated morphology of axon extension (Fig. 3d). In addition, the locations of the NMJs were marked by AChR-specific staining, further confirming the mutual binding site of the two cell types (Fig. 3e).

HUVECs were used to construct the aligned capillary-like network. Red fluorescent protein was used for cell labeling and tracking. The alignment of cells in a specific direction was observed under microscopy (Fig. 3f). Furthermore, staining of the F-actin cytoskeleton revealed its fused reticular morphology, confirming the mature appearance of the synthesized structures (Fig. 3g). Subsequently, both structures were transferred and stacked using photocurable hydrogel to assemble the aligned "sandwich" structure, with the neuromuscular layer on the upper and lower layers enveloping the middle vascular layer (Fig. 3h).

3.5 Craniofacial VML healing by the engineered tissue

We established a craniofacial VML model in nude mice by surgically removing approximately 40%–50% of the masseter muscle volume (Fig. 4a). This critical muscle defect does not heal spontaneously and can cause persistent muscle atrophy and dysfunction. We selected appropriately sized constructs based on the defective size and morphology and implanted them along the same direction. Furthermore, the Non-align, Sham, and Defect groups were collectively set as the control group. Figure 4b demonstrates the entire surgical procedure.

After four weeks of restoration, the histological structure of the masseter in all groups was analyzed by H&E and MT staining. The Defect group exhibited significant muscle atrophy and fiber degeneration, whereas the Align and Non-align groups showed increased muscle volume (Fig. 4e). Although the Non-align group showed partial muscle repair, the fiber distribution was disordered (Fig. 4c). Notably, in the Align group, the regenerated muscle fibers were regular in shape, with predominant alignment along the same direction (Fig. S2 in the supplementary information), and exhibited a smaller fibrous scar area, indicating better muscle repair ability (Figs. 4d and 4f). In addition, the hydrogel implanted in the defect site integrated with the original muscle and showed substantial degradation (Fig. S3 in the supplementary information), verifying the effective biocompatibility and biodegradability of the constructed tissue.

3.6 Evaluation of in vivo composite tissue regeneration

To clarify the impact of the construct on the composite muscle, nerve, and vessel tissue, we analyzed the specific markers of MHC, βIIIT, AChR, and platelet endothelial cell adhesion molecule-1 (CD31), in the repaired tissue of each group. The evaluation criteria for the muscle tissue structure based on histological staining results assessed muscle tissue morphology, size of muscle fibers, arrangement of muscle fibers, and distribution of fibrous tissue. Notably, the Align group exhibited a significant increase in MHC-positive (MHC+) myofiber area, and the morphology (size and arrangement) closely resembled that of the Sham group (Figs. 5a and 5b). Furthermore, the newly formed muscle fibers in the Align group showed distinct boundaries. The areas of the neuronal differentiation marker βIIIT and the NMJ-related marker AChR were increased in the Align group, both indicating better neural innervation (Figs. 5c and 5d; Fig. S4 in the supplementary information). Furthermore, an increase in CD31-positive (CD31+) vascular lumen was observed in the Align group, indicating the ability of

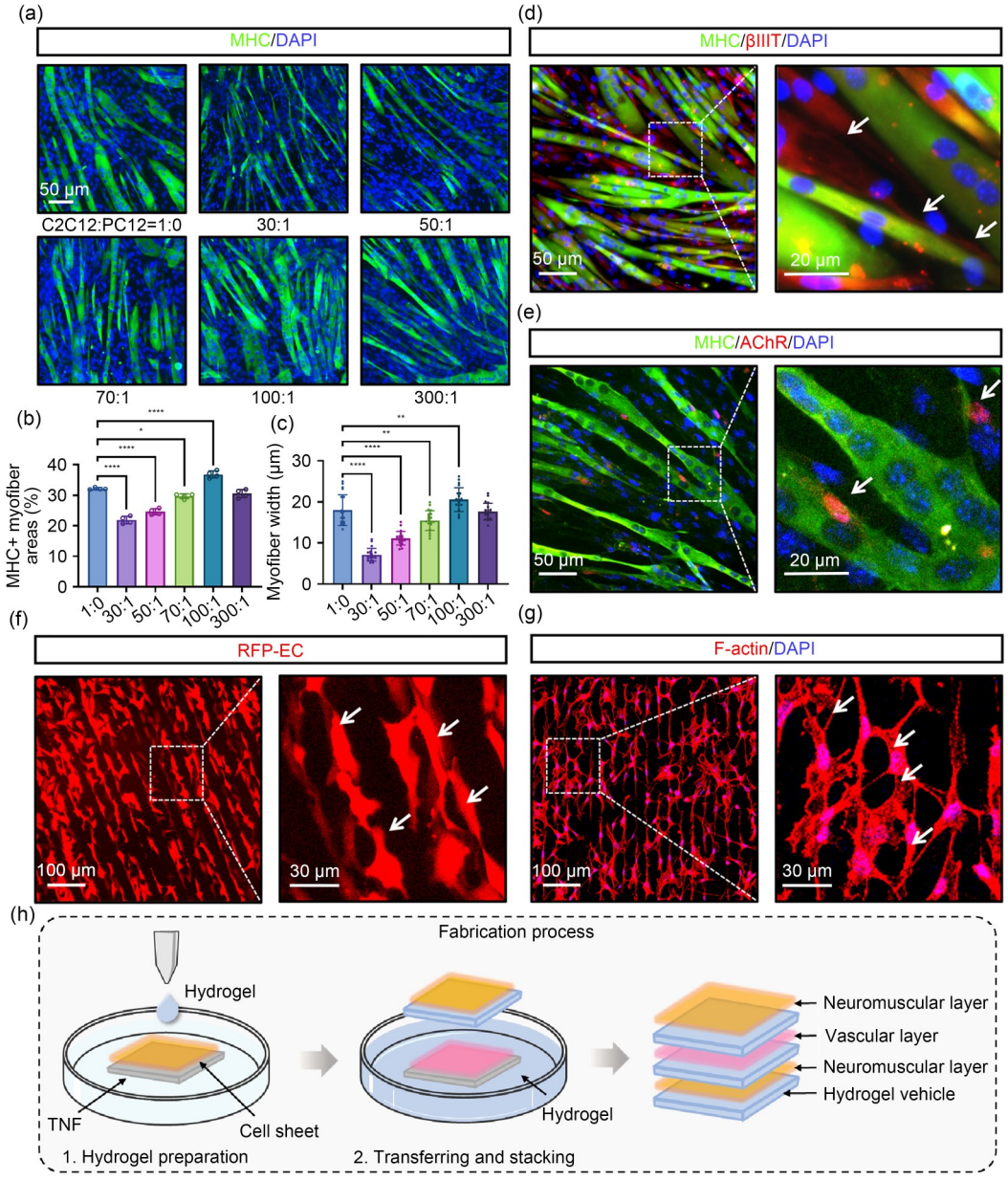

Fig. 3 Construction of aligned neurovascularized composite "sandwich" structure. (a) Immunofluorescence for MHC (green)/DAPI (blue) in C2C12 and PC12 cells mixed at different ratios during co-culture for 7 d in a 2D culture system. (b) Quantitative analysis of MHC+ myofiber areas among groups (n=4 per group). (c) Quantitative analysis of MHC+ myofiber widths (n=20 per group). (d) Double immunofluorescence for MHC (green)/βIIIIT (red)/DAPI (blue) in C2C12 and PC12 cells co-cultured at a 100∶1 ratio. White arrows indicate the differentiated morphology of neuronal axon extension. (e) Double immunofluorescence for MHC (green)/AChR (red)/DAPI (blue). White arrows indicate the location of AChR clustering and neuromuscular junctions. (f) Real-time fluorescence imaging of aligned capillary-like network formed by red fluorescent protein-labeled HUVECs. (g) Immunofluorescence for F-actin (red)/DAPI (blue). White arrows indicate the capillary-like reticular structure. (h) Diagram of the fabrication process of the composite "sandwich" structure. All data are expressed as mean±standard deviation; $^{*}p<0.05$, $^{**}p<0.01$, $^{****}p<0.0001$; ANOVA was employed followed by Tukey's test. RFP-EC: red fluorescent protein-labeled endothelial cell

engineered tissue to promote new blood vessel formation in vivo (Figs. 5e and 5f). Antibodies from distinct species used to label the nerves and vessels of both host and engineered tissues revealed areas of mutual integration and co-localization (Figs. 5g and 5i). The results of double-staining immunofluorescence confirmed the ability of the engineered tissue to integrate with the host tissue, with more integration sites in the Align group than in the Non-align group (Figs. 5h and 5j).

3.7 Functional evaluation

To evaluate the recovery of masseter function among the groups, we measured the food intake per unit time and

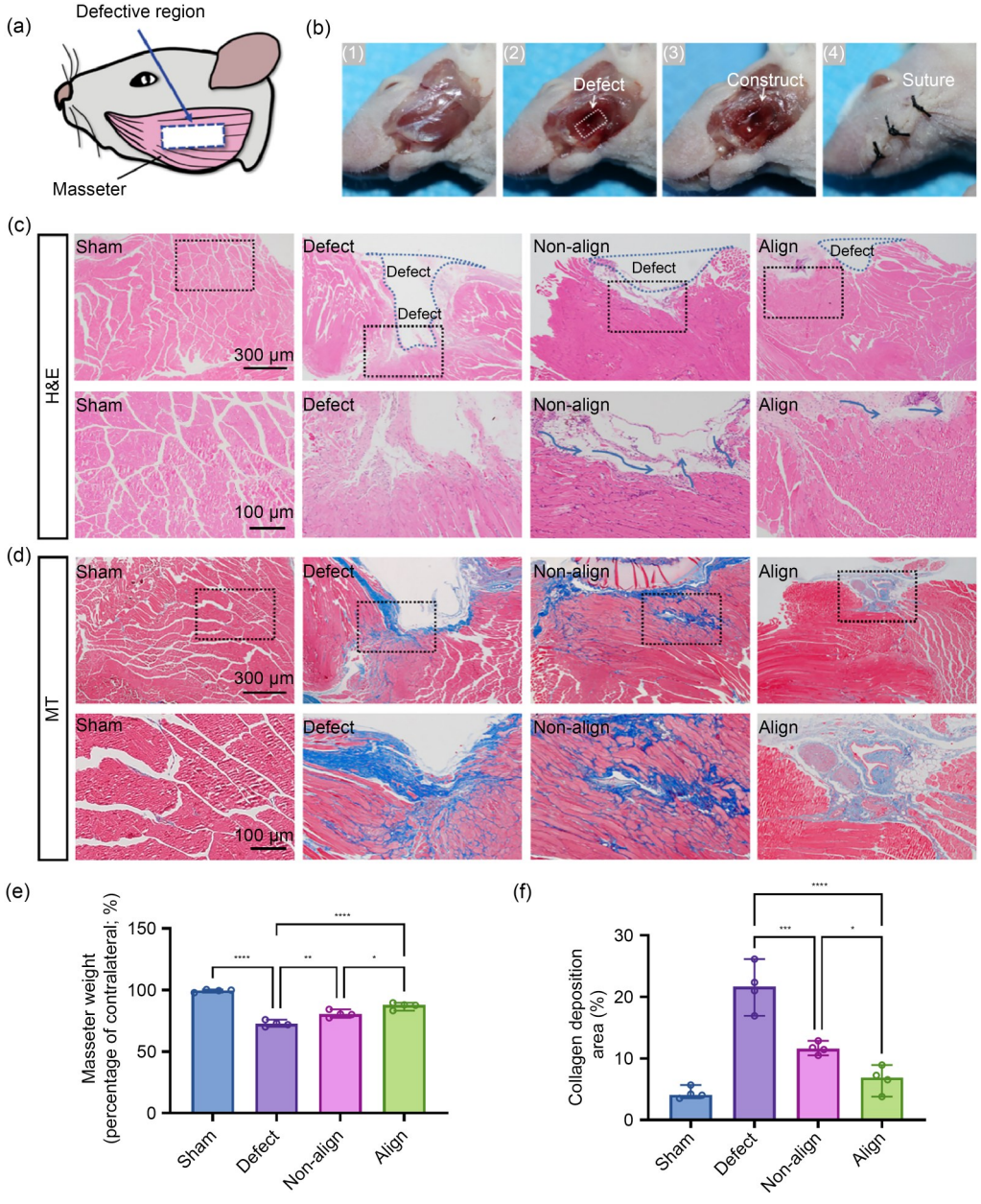

Fig. 4 Composite neurovascularized engineered muscle tissue implantation promotes the restoration of masseter muscle. (a) Schematic illustration of the defective region of the masseter muscle in a mouse. (b) Surgical establishment of the masseter defect and implantation of the engineered tissue. H&E (c) and MT (d) staining of the surgical areas four weeks after implantation (n=4 per group; black dashed box: enlarged area; blue dashed box: defective area; arrow: direction of the newly formed muscle fibers; blue stained area: fibrous scar tissue). (e) Quantification of masseter muscle mass (percentage of contralateral normal muscle) four weeks after implantation. (f) Quantification of the collagen deposition area based on MT staining (n=4 per group). All data are expressed as mean±standard deviation, $^{*}p<0.05$, $^{**}p<0.01$, $^{***}p<0.001$, $^{****}p<0.0001$; ANOVA was employed followed by Tukey's test

body weight changes in mice after four weeks of restoration. We found a considerable decrease in both body weight and food intake in the Defect group. Although the Non-align group showed an increased trend in food intake and body weight, no significant difference was found compared to the Defect group. Notably, the Align group demonstrated significantly higher food intake and body weight, confirming better functional recovery in this group than in the others (Figs. S5a and S5b in the supplementary information).

4 Discussion

The masseter muscle is a crucial component of the craniofacial musculature that functions in mastication and phonation.

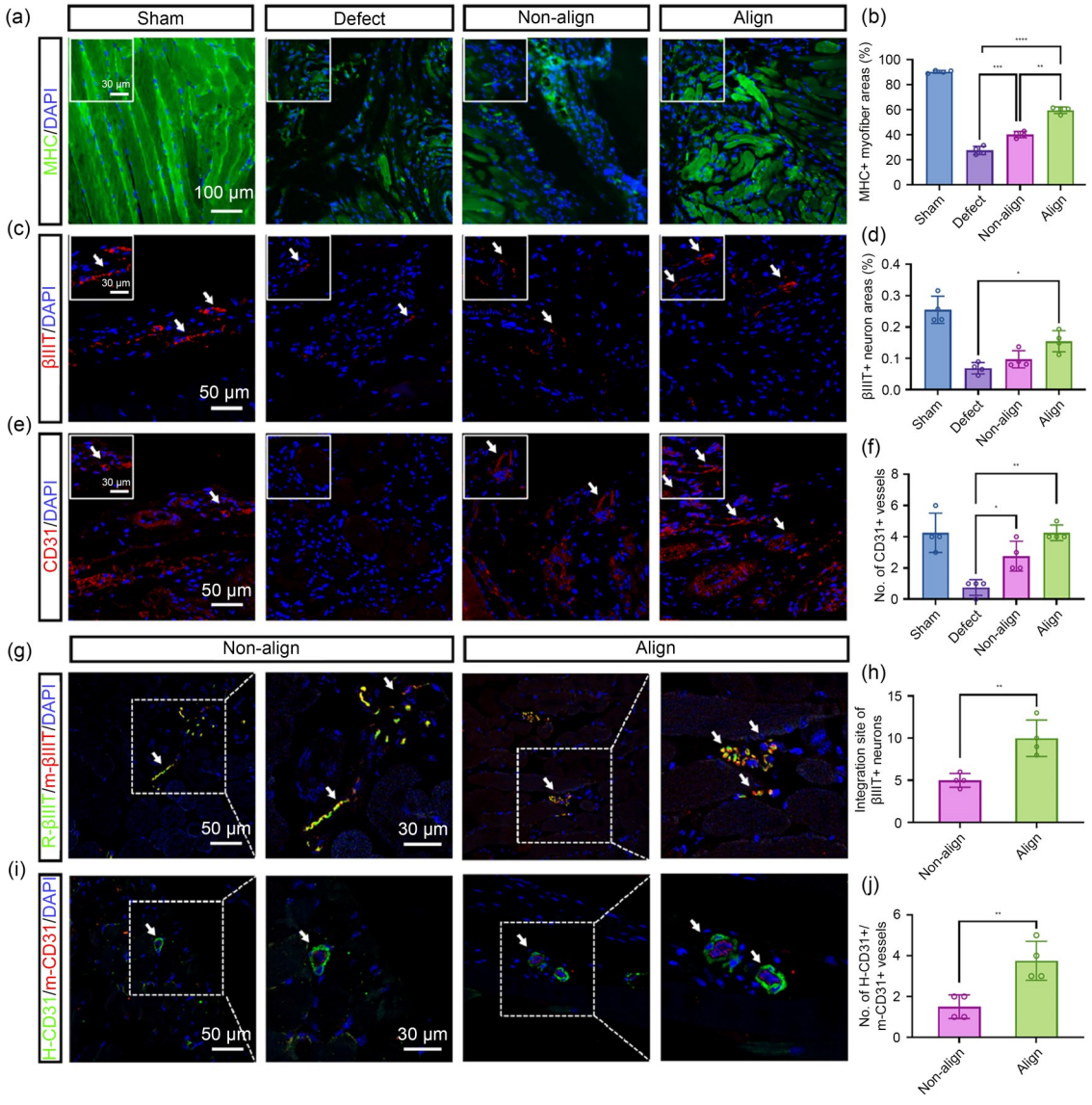

Fig. 5 Composite tissue regeneration in the masseter muscle region after four weeks of restoration. (a) Immunofluorescence for myogenic marker MHC (green)/DAPI (blue) of the surgically removed area of masseter muscle after four weeks of restoration. White squares: magnified image of the target area. (b) Quantification of the areas of MHC+ myofibers. (c) Immunofluorescence for neural marker βIIIT (red)/DAPI (blue) of the surgical area. White arrows indicate βIIIT+ neurons. (d) Quantification of the areas of βIIIT+ neurons. (e) Immunofluorescence for vascular marker CD31 (red)/DAPI (blue) of the surgical area. White arrows indicate CD31+ vascular lumens. (f) Quantification of the numbers of CD31+ vascular lumens. (g) Immunofluorescence for βIIIT of rat species (R-βIIIT) labeled as the implanted tissue (green) and of mouse species (m-βIIIT) labeled as the host tissue (red), and for DAPI (blue). (h) Quantification of the integration site of R-βIIIT+/m-βIIIT+ neurons. (i) Immunofluorescence for CD31 of human species (H-CD31; green) and of mouse species (m-CD31; red), and for DAPI (blue). (j) Quantification of the number of H-CD31+/m-CD31+ vessels (n=4 per group). All data are expressed as mean±standard deviation, $^{*}p<0.05$, $^{**}p<0.01$, $^{***}p<0.001$, $^{****}p<0.0001$; ANOVA was employed followed by Tukey's test. βIIIT+: βIIIT-positive; CD31+: CD31-positive

However, substantial defects sustained from trauma or surgical procedures can lead to craniofacial VML, which causes severe muscular functional impairment and facial deformities [24–26]. Numerous studies on muscle tissue engineering have focused on the reconstruction of large-scale skeletal muscle defects [27–29]. However, limited attention has been given to craniofacial musculature. Recent muscle reconstruction strategies have explored the development of biocompatible scaffolds with various properties to emulate the physiological characteristics of natural tissues [30, 31]. These approaches include the construction of ordered scaffolds to facilitate the directional alignment of muscle fibers [32], enhancement of the strength and stiffness of scaffolds to match natural tissues [33], and simulation of muscle contraction activities [34]. By simulating normal structural features, these methods encourage muscle ingrowth by inducing microenvironments or by acting as a cell delivery vehicle [35]. However, these strategies exhibit

limited capacity for the repair of surrounding nerves and blood vessels. Furthermore, functional recovery deficits may be primarily caused by the limited rate and extent of vascularization and neural innervation of the implanted engineered tissue, causing the engineered muscle to atrophy before it becomes functionally integrated with surrounding host tissues [36].

Denervation has long been disregarded in VML pathophysiology. VML can disrupt motor neurons and NMJs, altering the innervation of skeletal muscles and causing acute denervation of muscle fibers within the remaining muscle tissue and progressive deterioration within six months [37]. In addition, investigations on spinal cord and peripheral nerve injury have demonstrated that innervation is intimately linked to muscle contractility and the excitation–contraction coupling [38, 39], which can promote the restoration of muscle strength. Among these, NMJs may be a critical site for signal transmission and the re-establishment of innervation inside muscle tissue. NMJs serve as a specialized interface between motor neurons and their innervated skeletal muscle fibers, converting action potentials from motor neurons into effective muscle contractions [40]. Muscle fibers undergo membrane depolarization, voltage-gated calcium channels open, and intracellular calcium levels increase in response to motor neuron action potentials and subsequent acetylcholine release, thereby activating the contractile apparatus [41]. These studies have provided further evidence for our in vitro reconstruction of NMJs and the successful innervation of muscle tissue.

Our findings indicate that the addition of a small proportion of PC12 cells effectively accelerated myogenic differentiation and the formation of NMJs through neuromuscular co-culture. Co-cultured cells can promote intercellular signal transmission and activate intracellular signal transduction pathways through direct cellular contact [42]. Moreover, neural cells are capable of producing and releasing various growth factors and neurotrophic factors, including nerve growth factor, glial cell line-derived neurotrophic factor, and neuropeptides [43], which can stimulate myoblasts to proliferate and differentiate. The addition of PC12 cells may have also altered the microenvironment in the co-culture system, creating conditions more conducive to myogenic differentiation. While the addition of a small number of PC12 cells can accelerate myogenesis, the introduction of a large number of non-myogenic cells can conversely hinder the fusion and differentiation of myoblasts [44], thus emphasizing the use of an appropriate cell co-culture ratio.

In this study, we employed an accessible and feasible approach for controlling the directional alignment of muscle cells, resulting in the construction of mature-oriented muscle fibers and thereby enhancing unidirectional muscle contraction force. Simultaneously, we established a neuron–myoblast in vitro co-culture system to elucidate the interaction between nerve and muscle cells, which confirmed the feasibility of establishing NMJs in vitro. Additionally, we implemented a pre-vascularization strategy to enhance the post-transplantation survival of engineered tissue and mitigate tissue hypoxia [45]. Using hydrogels as the assembly matrix not only effectively retained extracellular matrix cues but also circumvented a range of issues associated with implanting scaffolds, including biocompatibility and degradation concerns. Moreover, the presence of scar tissue is a crucial factor in the recovery of muscle function. Scar tissue, which lacks the elasticity and contractility of muscle tissues, can impair function when accumulated excessively, affecting muscle flexibility and strength. By enhancing muscle regeneration efficiency and reducing scar tissue formation, our treatment approach has facilitated significant functional tissue regeneration and achieved satisfactory results, presenting a promising therapeutic option for the functional regeneration of craniofacial muscles.

While this research describes the development of a novel therapeutic approach in reconstructive surgery, its biosafety and long-term efficacy require further evaluation in practical applications. Future studies should focus on enhancing technical aspects and advancing clinical translation. Moreover, the interactions among muscles, nerves, and blood vessels should be explored to uncover their specific mechanisms of action.

Supplementary Information The online version contains supplementary material available at https://doi.org/10.1631/bdm.2400005.

Acknowledgements This work was financially supported by the National Natural Science Foundation of China (Nos. 82122014, 82071085, 82020108011, and 82301031), the Zhejiang Provincial Natural Science Foundation of China (No. LR21H140001), the National Key Research and Development Program of China (No. 2018YFA0703000), the Medical Technology and Education of Zhejiang Province of China (No. 2018KY501), and the Fundamental Research Funds for the Central Universities (No. 2022QZJH55).

Author contributions SJD and SJL: conceptualization and design, collection and assembly of data, data analysis and interpretation, and manuscript writing; ZJS and XW: material production and data analysis; YHC: manuscript revision and literature collection; JXH, HMW, and MFY: conceptualization and design, financial support, administrative support, manuscript revision, and final approval of the manuscript. All authors have read and approved the final manuscript.

Declarations

Conflict of interest MFY is an associate editor for *Bio-Design and Manufacturing* and was not involved in the editorial review or the decision to publish this article. The authors declare that they have no conflict of interest.

Ethical approval This project was approved by Zhejiang University Animal Care and Use Committee. The approval code number is ZJU20230192. All institutional and national guidelines for the care and use of laboratory animals were followed.

Data availability All data generated or analyzed during this study are available in the main text or the supplementary materials.

References

1. Janssen I, Heymsfield SB, Wang ZM et al (2000) Skeletal muscle mass and distribution in 468 men and women aged 18–88 yr. J Appl Physiol 89(1):81–88. https://doi.org/10.1152/jappl.2000.89.1.81
2. Wang ZL, Yang JJ, Sun XH et al (2023) Exosome-mediated regulatory mechanisms in skeletal muscle: a narrative review. J Zhejiang Univ Sci B (Biomed & Biotechnol) 24(1):1–14. https://doi.org/10.1631/jzus.B2200243
3. Bailey P, Holowacz T, Lassar AB (2001) The origin of skeletal muscle stem cells in the embryo and the adult. Curr Opin Cell Biol 13(6):679–689. https://doi.org/10.1016/s0955-0674(00)00271-4
4. Mootoosamy RC, Dietrich S (2002) Distinct regulatory cascades for head and trunk myogenesis. Development 129(3): 573–583. https://doi.org/10.1242/dev.129.3.573
5. Schubert FR, Singh AJ, Afoyalan O et al (2019) To roll the eyes and snap a bite – function, development and evolution of craniofacial muscles. Semin Cell Dev Biol 91:31–44. https://doi.org/10.1016/j.semcdb.2017.12.013
6. Wachtler F, Jacob M (1986) Origin and development of the cranial skeletal muscles. Bibliotheca Anatomica 29:24–46
7. Isola G, Anastasi GP, Matarese G et al (2018) Functional and molecular outcomes of the human masticatory muscles. Oral Dis 24(8):1428–1441. https://doi.org/10.1111/odi.12806
8. Shirakawa T, Miyawaki A, Kawamoto T et al (2021) Natural compounds attenuate denervation-induced skeletal muscle atrophy. Int J Mol Sci 22(15):8310. https://doi.org/10.3390/ijms22158310
9. Garg K, Ward CL, Hurtgen BJ et al (2015) Volumetric muscle loss: persistent functional deficits beyond frank loss of tissue. J Orthop Res 33(1):40–46. https://doi.org/10.1002/jor.22730
10. L'Heureux N, Letourneur D (2015) Clinical translation of tissue-engineered constructs for severe leg injuries. Ann Trans Med 3(10):134. https://doi.org/10.3978/j.issn.2305-5839.2015.05.03
11. Aguilar CA, Greising SM, Watts A et al (2018) Multiscale analysis of a regenerative therapy for treatment of volumetric muscle loss injury. Cell Death Discov 4(1):33. https://doi.org/10.1038/s41420-018-0027-8
12. Gholobova D, Terrie L, Gerard M et al (2020) Vascularization of tissue-engineered skeletal muscle constructs. Biomaterials 235:119708. https://doi.org/10.1016/j.biomaterials.2019.119708
13. Daigeler A, Drücke D, Tatar K et al (2009) The pedicled gastrocnemius muscle flap: a review of 218 cases. Plast Reconstr Surg 123(1):250–257. https://doi.org/10.1097/PRS.0b013e3181904e2e
14. Ono Y, Boldrin L, Knopp P et al (2010) Muscle satellite cells are a functionally heterogeneous population in both somite-derived and branchiomeric muscles. Dev Biol 337(1):29–41. https://doi.org/10.1016/j.ydbio.2009.10.005
15. Pavlath GK, Thaloor D, Rando TA et al (1998) Heterogeneity among muscle precursor cells in adult skeletal muscles with differing regenerative capacities. Dev Dyn 212(4):495–508. https://doi.org/10.1002/(SICI)1097-0177(199808)212:4<495::AID-AJA3>3.0.CO;2-C
16. Furusawa K, Kawahana Y, Miyashita R (2023) Construction of engineered muscle tissue consisting of myotube bundles in a collagen gel matrix. Gels 9(2):141. https://doi.org/10.3390/gels9020141
17. Shadrach JL, Wagers AJ (2011) Stem cells for skeletal muscle repair. Philos T R Soc B 366(1575):2297–2306. https://doi.org/10.1098/rstb.2011.0027
18. McComas AJ (1998) Oro-facial muscles: internal structure, function and ageing. Gerodontology 15(1):3–14. https://doi.org/10.1111/j.1741-2358.1998.00003.x
19. Bongers KS, Fox DK, Ebert SM et al (2013) Skeletal muscle denervation causes skeletal muscle atrophy through a pathway that involves both Gadd45a and HDAC4. Am J Physiol Endocrinol Metabol 305(7):E907–E915. https://doi.org/10.1152/ajpendo.00380.2013
20. Adidharma W, Khouri AN, Lee JC et al (2022) Sensory nerve regeneration and reinnervation in muscle following peripheral nerve injury. Muscle Nerve 66(4):384–396. https://doi.org/10.1002/mus.27661
21. Adams RH, Alitalo K (2007) Molecular regulation of angiogenesis and lymphangiogenesis. Nat Rev Mol Cell Biol 8(6): 464–478. https://doi.org/10.1038/nrm2183
22. Luo M, Cheng K, Weng WJ et al (2009) Size- and density-controlled synthesis of TiO_2 nanodots on a substrate by phase-separation-induced self-assembly. Nanotechnology 20(21):215605. https://doi.org/10.1088/0957-4484/20/21/215605
23. Liu C, Zhou Y, Sun M et al (2017) Light-induced cell alignment and harvest for anisotropic cell sheet technology. ACS Appl Mater Interfaces 9(42):36513–36524. https://doi.org/10.1021/acsami.7b07202
24. Lew TA, Walker JA, Wenke JC et al (2010) Characterization of craniomaxillofacial battle injuries sustained by United States service members in the current conflicts of Iraq and Afghanistan. J Oral Maxillofac Surg 68(1):3–7. https://doi.org/10.1016/j.joms.2009.06.006
25. Gassner R, Tuli T, Hächl O et al (2003) Cranio-maxillofacial trauma: a 10 year review of 9,543 cases with 21,067 injuries. J Cranio-maxillo-facial Surg 31(1):51–61. https://doi.org/10.1016/S1010-5182(02)00168-3
26. De Sousa A (2008) Psychological issues in oral and maxillofacial reconstructive surgery. Brit J Oral Maxillofac Surg 46(8): 661–664. https://doi.org/10.1016/j.bjoms.2008.07.192
27. Jana S, Cooper A, Zhang MQ (2013) Chitosan scaffolds with unidirectional microtubular pores for large skeletal myotube generation. Adv Healthc Mater 2(4):557–561. https://doi.org/10.1002/adhm.201200177
28. Chen SW, Nakamoto T, Kawazoe N et al (2015) Engineering multi-layered skeletal muscle tissue by using 3D microgrooved collagen scaffolds. Biomaterials 73:23–31. https://doi.org/10.1016/j.biomaterials.2015.09.010
29. Kroehne V, Heschel I, Schügner F et al (2008) Use of a novel collagen matrix with oriented pore structure for muscle cell differentiation in cell culture and in grafts. J Cell Mol Med 12(5a): 1640–1648. https://doi.org/10.1111/j.1582-4934.2008.00238.x
30. Zhang B, Xue Q, Hu HY et al (2019) Integrated 3D bioprinting-based geometry-control strategy for fabricating corneal substitutes. J Zhejiang Univ Sci B (Biomed & Biotechnol) 20(12): 945–959. https://doi.org/10.1631/jzus.B1900190
31. Aazmi A, Guo ZX, Yu HR et al (2023) Enhanced mixing efficiency for a novel 3D Tesla micromixer for Newtonian and non-Newtonian fluids. J Zhejiang Univ Sci A (Appl Phys & Eng)

24(12):1065–1078.
https://doi.org/10.1631/jzus.A2300589
32. Guan JJ, Fujimoto KL, Wagner WR (2008) Elastase-sensitive elastomeric scaffolds with variable anisotropy for soft tissue engineering. Pharm Res 25(10):2400–2412.
https://doi.org/10.1007/s11095-008-9628-x
33. Christensen KW, Turner J, Coughenour K et al (2022) Assembled cell-decorated collagen (AC-DC) fiber bioprinted implants with musculoskeletal tissue properties promote functional recovery in volumetric muscle loss. Adv Healthc Mater 11(3):e2101357.
https://doi.org/10.1002/adhm.202101357
34. Zhao LL, Zhang X, Luo Q et al (2020) Engineering nonmechanical protein-based hydrogels with highly mechanical properties: comparison with natural muscles. Biomacromolecules 21(10): 4212–4219.
https://doi.org/10.1021/acs.biomac.0c01002
35. Wolf MT, Dearth CL, Sonnenberg SB et al (2015) Naturally derived and synthetic scaffolds for skeletal muscle reconstruction. Adv Drug Deliv Rev 84:208–221.
https://doi.org/10.1016/j.addr.2014.08.011
36. Rousseau E, Raman R, Tamir T et al (2023) Actuated tissue engineered muscle grafts restore functional mobility after volumetric muscle loss. Biomaterials 302:122317.
https://doi.org/10.1016/j.biomaterials.2023.122317
37. Sorensen JR, Hoffman DB, Corona BT et al (2021) Secondary denervation is a chronic pathophysiologic sequela of volumetric muscle loss. J Appl Physiol 130(5):1614–1625.
https://doi.org/10.1152/japplphysiol.00049.2021
38. Sulaiman W, Gordon T (2013) Neurobiology of peripheral nerve injury, regeneration, and functional recovery: from bench top research to bedside application. Ochsner J 13(1):100–108
39. Kern H, Boncompagni S, Rossini K et al (2004) Long-term denervation in humans causes degeneration of both contractile and excitation-contraction coupling apparatus, which is reversible by functional electrical stimulation (FES): a role for myofiber regeneration? J Neuropath Exp Neur 63(9):919–931.
https://doi.org/10.1093/jnen/63.9.919
40. Lin CY, Yoshida M, Li LT et al (2019) iPSC-derived functional human neuromuscular junctions model the pathophysiology of neuromuscular diseases. JCI Insight 4(18):e124299.
https://doi.org/10.1172/jci.insight.124299
41. Kuo IY, Ehrlich BE (2015) Signaling in muscle contraction. CSH Perspect Biol 7(2):a006023.
https://doi.org/10.1101/cshperspect.a006023
42. Kuppusamy P, Kim D, Soundharrajan I et al (2020) Adipose and muscle cell co-culture system: a novel in vitro tool to mimic the in vivo cellular environment. Biology 10(1):6.
https://doi.org/10.3390/biology10010006
43. Narayanan N, Lengemann P, Kim KH et al (2021) Harnessing nerve-muscle cell interactions for biomaterials-based skeletal muscle regeneration. J Biomed Mater Res Part A 109(3):289–299.
https://doi.org/10.1002/jbm.a.37022
44. Kim JH, Kim I, Seol YJ et al (2020) Neural cell integration into 3D bioprinted skeletal muscle constructs accelerates restoration of muscle function. Nat Commun 11(1):1025.
https://doi.org/10.1038/s41467-020-14930-9
45. Sun HY, Ma HY, Wang L et al (2024) Biomimetic microchannel network with functional endothelium formed by sacrificial electrospun fibers inside 3D gelatin methacryloyl (GelMA) hydrogel models. J Zhejiang Univ Sci A (Appl Phys & Eng) 25(1):79–96.
https://doi.org/10.1631/jzus.A23D0045